s

Single EGF mutants unravel the mechanism for stabilization of Epidermal Growth Factor Receptor (EGFR) system

Stefano Pascarelli[1], Dalmira Merzhakupova[1], Gen-Ichiro Uechi[1], Paola Laurino[1*]

[1] Okinawa Institute of Science and Technology Graduate University, 1919-1 Tancha, Onna-son, Okinawa 904-0495 Japan.

* Corresponding author

E-mail: paola.laurino@oist.jp

Abstract

The Epidermal Growth Factor Receptor (EGFR) is a membrane-anchored tyrosine kinase that is able to respond to multiple extra-cellular stimuli in a selective way. Previous studies have pointed out that the modularity of this system could be carried out by ligand-induced differences in the stability of the dimerized receptor. However, nobody has ever explored this hypothesis by observing the effects of single-mutant ligands so far.

Herein, we generated single mutants after we identified positions responsible of inducing functional divergence among paralog ligands using a newly developed approach. Then, we assessed the mutants' effects on the receptor by employing a combination of molecular dynamics and experimental techniques. Although having comparable binding affinities for EGFR to the wild type, the mutants induced different responses at both the receptor and the cellular level. This study shows for the first time that a functional transition in EGFR can be imparted with as little as one targeted mutation on the ligand. These results also support the theory of biased signaling in the tyrosine kinase receptor system.

Abbreviations

EGF, Epidermal Growth Factor

EGFR, Epidermal Growth Factor Receptor

PPI, Protein-Protein Interaction

MSA, Multiple Sequence Alignment

MSTA, Multiple STructural Alignment

ITC, Isothermal Titration Calorimetry

DMEM, Dulbecco's Modified Eagle Medium

ECD, Extra Cellular Domain

WT, Wild Type

CD, circular dichroism

Introduction

The Epidermal Growth Factor (EGF)-like domain ligand-receptor signaling system is involved in many biological events in multicellular organisms (1). This system is constituted by one receptor (EGFR) and seven distinct peptide ligands (EGF, HBEGF, EPGN, BTC, EREG, AREG, TGFA). Upon binding to the receptor, these ligands can activate multiple intracellular downstream pathways through an interaction network with a bow-tie structure (2). For all ligands, binding induces a transition from monomer or inactive dimer to an active dimer state (3, 4). However, different ligands are able to promote divergent outcomes, even at saturating concentrations; thus, the mechanism responsible of the modular downstream pathway activation is independent of ligand affinity or potency, and likely encompasses intrinsic effects (5). It is well known that the EGFR system play a key role in cancer development. In particular, some studies have shown that overexpression of EGFR or its ligands may induce different types of cancer (6). A better understanding of the interaction between EGFR and its ligands could lead to the development of targeted therapies (7).

Protein-protein interactions (PPIs), such as that between EGFR and its ligands, are some of the most interesting and well-studied examples of molecular co-evolution in biological systems. These interactions are sometimes defined by one part (receptor) that binds several counterparts (ligands). In these instances, receptors and ligands experience different selective constraints, where receptors tend to evolve more slowly due to the necessity of binding multiple ligands (8). Furthermore, paralogs, proteins related by a duplication event, are less

likely to retain the same function as orthologs, proteins related by a speciation event (9). Then, paralogous ligands rather than the receptor are a good candidate to test the functional divergence in the biased signaling system. However, this approach is susceptible to indirect factors that get into play. For example, not all ligands might have the same binding selectivity, thus resulting in the activation of unrelated pathways. In this work, we decided to test single mutants of one ligand, EGF, by identifying and modifying sites responsible for a divergent function among paralog ligands. In recent years, different experimental techniques have been developed to define the effects of single mutant proteins at the cellular level (10). Recent studies have shown that some EGF residues like Arg-41 and Leu-47 are highly conserved and important for high binding affinity to EGFR (11). Another study highlighted Tyr-13, Leu-15 and His-16 in EGF as essential for downstream activity of ErbB1 (12). These outcomes were based on structural analyses of ligands and experimental validation. While bioinformatic tools such as contact prediction (13) or molecular dynamics (14) can give a good overall picture of ligand-receptor interactions, the contribution of single ligand residues to the modularity of the system still remains unclear.

Ligand-induced selective activation of downstream pathway has been observed in G-protein coupled receptors, a phenomenon known as “biased signaling” (15, 16). A recent report hints that this mechanism might also take place in EGFR tyrosine kinase (17). Initially, the main contributor to the modularity of the system was thought to be the affinity of the ligands to the receptor. However, the discovery of the ligand EPGN, which induces a potent mitogen effect despite low binding affinity (18), and multiple cell-line studies (5) have changed this perspective. The standing theory is that different EGFR ligands induce different receptor dimer stabilities, altering the phosphorylation dynamics; stable receptor dimers show transient activation, reaching the phosphorylation level required to initiate negative feedback

signals faster than the unstable counterparts (19). Now, the open question is how these ligands induce different dimer stabilities. Interactions between the interface of the ligand and EGFR have been shown to influence the stability of the dimerized receptor (20), a factor that is related to ligand-specific signaling bias (19, 21). It is known that the EGFR dimer can be observed in a symmetrical, “flush” conformation or an asymmetrical, “staggered” conformation (22) depending on the presence/absence of the membrane, glycosylation, and the number of bound ligands (23). Whether and how this plays a role in biased signaling is still unknown.

Here we show how single amino acid substitutions alter biased signaling in the EGF-EGFR ligand-receptor system. We developed a new bioinformatic tool to analyze the co-evolution of the ligand-receptor pair and identify candidate function-altering mutations. The identified mutants induced an altered phosphorylation dynamics and different cellular phenotype. This is the first study to explain differences in biased signaling of EGFR using single-residue EGF mutants. Furthermore, our co-evolutionary analysis can be applied readily to other ligand-receptor interactions.

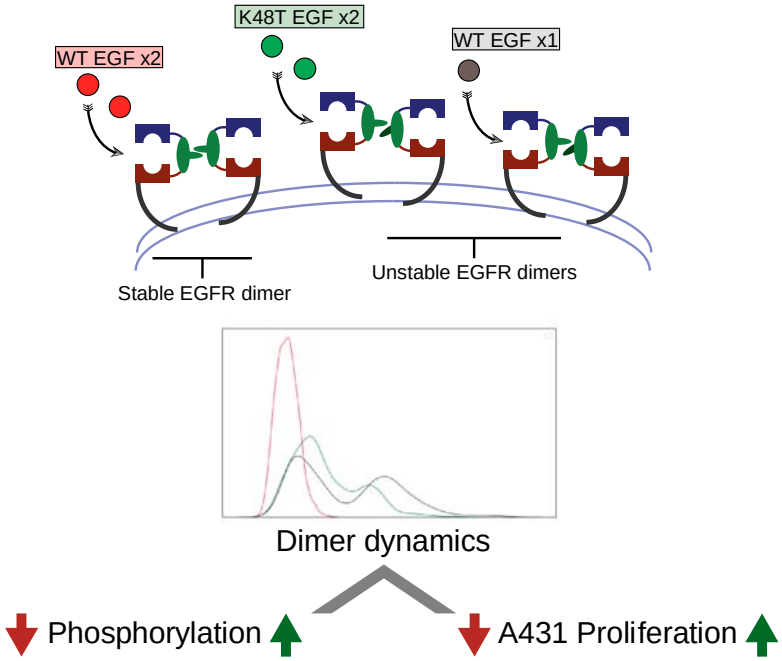

Figure 1. Study rationale. EGF K48T mutant was identified using an *ad hoc* methodology that combines conservation and coevolution measures. Unlike WT EGF, two K48T ligands induce an unstable conformation of the receptor dimer, similarly to a dimer with a single WT EGF. Treating A431 cells with either WT EGF or K48T mutant EGF resulted in a different response both in the phosphorylation dynamics and the cell proliferation phenotype.

Results

DIRpred

Firstly, we developed a method for predicting residues that are likely to be responsible for functional differences induced by paralogous ligands of a given receptor, which we called DIRpred (Divergence Inducing Residues prediction). Our approach combines residue-specific conservation measures to identify positions that are conserved among orthologs while diverging among paralogs. The DIRpred analysis is based on the assumption that conservation of a residue in orthologs of a specific ligand shows whether a residue is

important for either structural or functional reasons, while conservation of a residue among paralogous ligands denotes the importance of a residue for receptor binding (the main shared property of all ligands). Thus, residues that are highly conserved in orthologs but not paralogs of a ligand are likely related to the ligand's specific function. Unlike other existing methods for prediction of specificity determining residues (a review can be found in (24)), we included inter-protein coevolution measures to narrow down those residues that are responsible for a specific function. The DIRpred score is calculated as the sum of the four components (I: orthologs conservation, II: complement of the paralog's conservation, III: ligand-receptor co-evolution, IV: complement of ligand internal co-evolution). Optionally, the analysis can be conducted using a structural alignment of the paralogs instead of the sequence alignment.

DIRpred analysis of EGF

We applied the DIRpred algorithm to predict single amino acid substitutions in EGF that would alter its function (Figure 2). Since the analysis requires prior knowledge of paralogs and orthologs of the target gene, we first performed a phylogenetic analysis to confirm that the reported paralogous ligands of EGF are monophyletic (Supplementary figure 1). The DIRpred analysis highlighted residue Asn-32, Asp-46, Lys-48 and Trp-50 as potential candidates for paralog functional divergence. Asn-32 and Lys-48 show a very small conservation in both sequence and structure alignments resulting in a high partial score (II). Asp-46 has a relatively high coevolution with the receptor (III), while Trp-50 has high scores overall (Figure 2 — figure Supplement 1). We chose to introduce orthologous substitutions at these four positions, as orthologous have been previously observed as enriched in function (see Materials and Metods) (25). The four designed EGF mutants with a single amino-acid

substitution that were selected for functional characterization were N32R, D46T, K48T and W50Y.

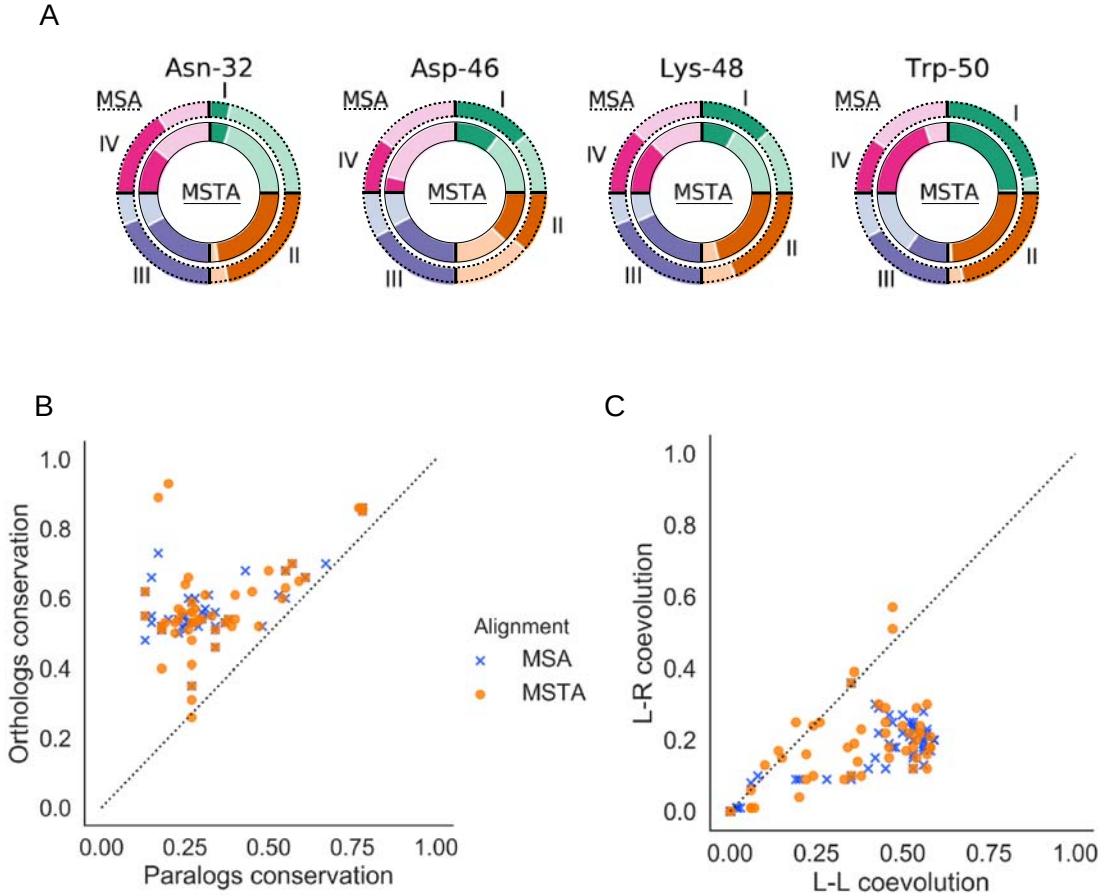

Figure 2. DIRpred analysis of EGF. (A) The relative ranking score of the four mutants. The outer circle represents paralogs MSA-based scores, while the inner circle represents paralogs MSTA-based scores. The darker color indicates a higher ranking in the EGF sites-based scoring. (B) Cross-conservation plot. The plot is obtained by crossing the two conservation scores. Interestingly, no point lies in the bottom right half of the plot (high paralogs conservation and low orthologs conservation), suggesting that paralogs and orthologs conservation are not independent. This observation points out that there is no organism-specific adaptation shared by all ligands at the protein sequence level. (C) Cross-co-evolution score. The plot is obtained by crossing the two co-evolution scores, the ligand-receptor (L-R)

co-evolution score (III) on the y axis and the ligand-ligand (L-L) co-evolution score (IV) on the x axis.

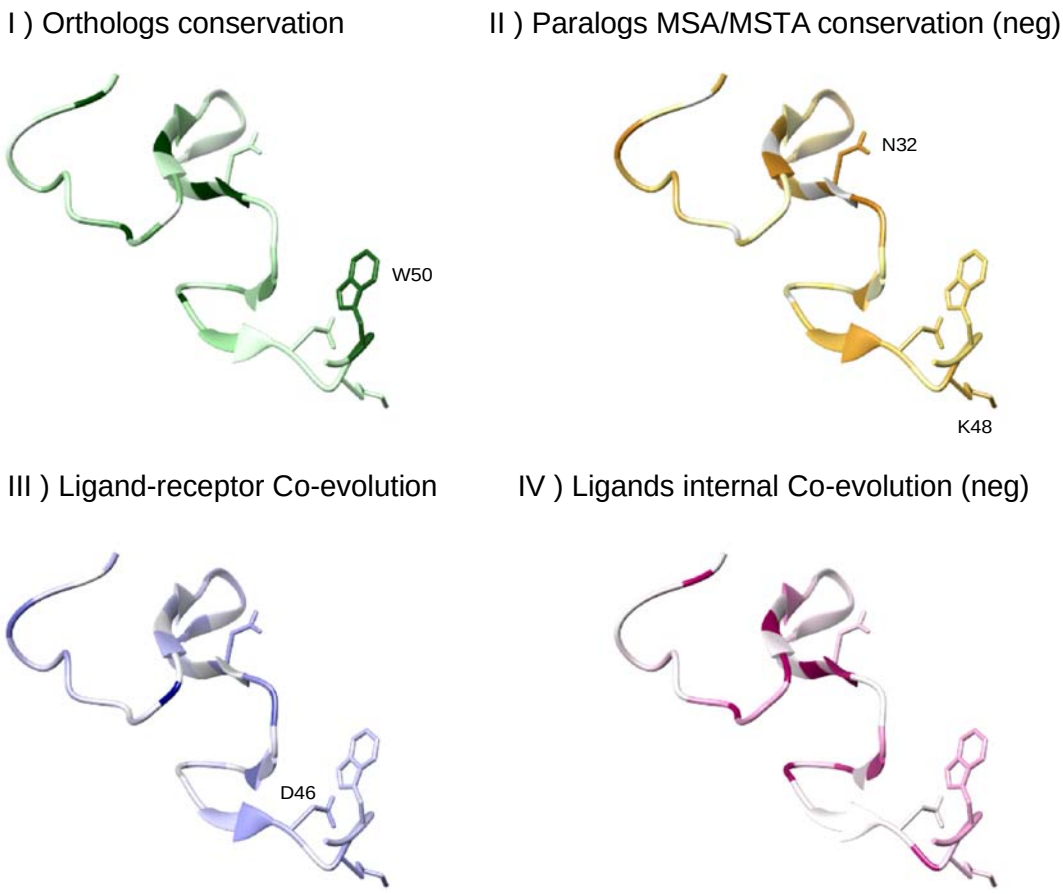

Figure 2—figure Supplement 1. DIRpred score. Structure of EGF (from PDB: 1IVO) colored by the four individual scores. The four sites chosen for mutation are shown in stick representation.

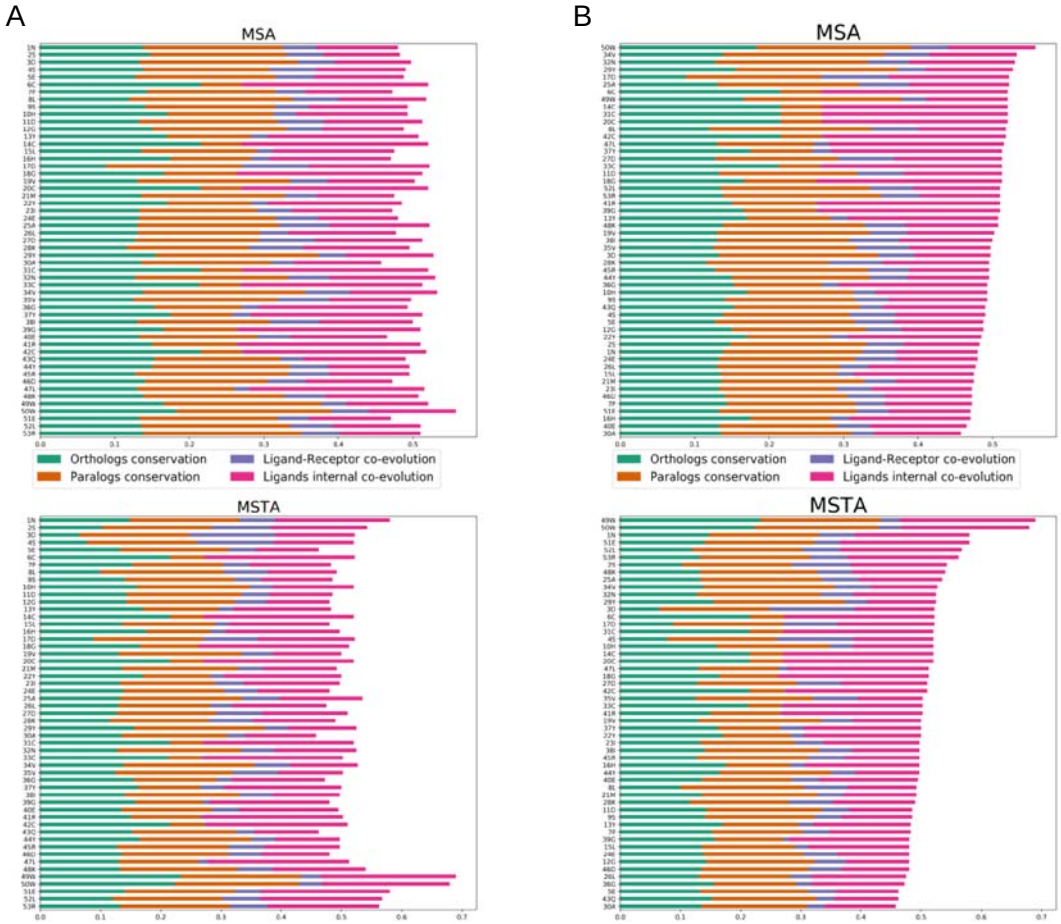

Figure 2—figure Supplement 2. All sites score. This figure shows the four scores for each site of EGF. On the top, the paralogs MSA based scores, while on bottom, scores are based on the paralogs MSTA. In (A) the scores are in order of sequence. In (B), the scores are sorted by highest sum first.

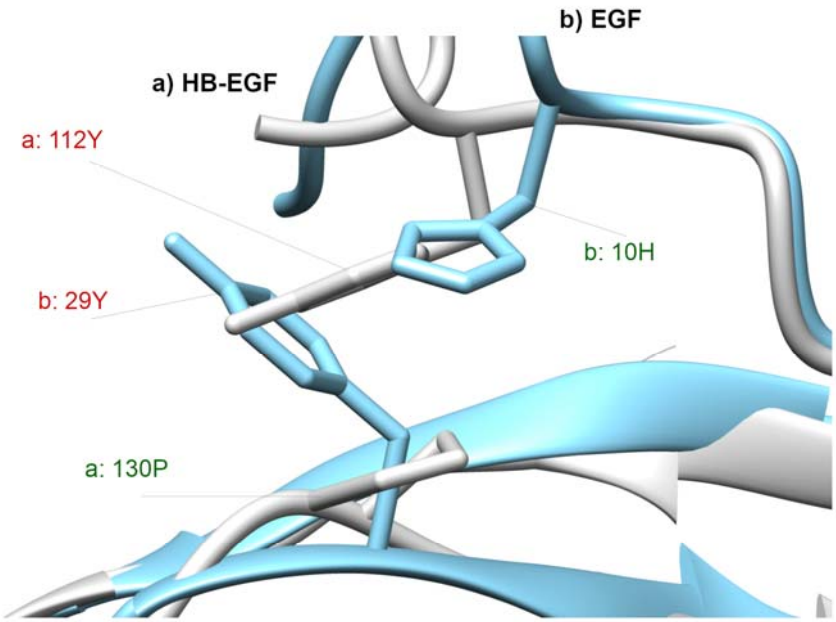

Figure 2—figure Supplement 3. Highlight on the EGF-specific residue swapping problem. EGF is colored in teal, while HB-EGF is colored in white. The tyrosine in EGF position 29 (29Y) is not found on the corresponding position of HB-EGF. Instead, a proline is found (130P). Though, the interaction between the two residue is probably maintained because, in place of the histidine 10 (10H) of EGF, HB-EGF shows a tyrosine (112Y). When this type of residue swapping is ligand-specific, the lowering of the conservation measures over-estimates the real change happening in that position.

Biochemical properties of the EGF mutants

To determine the functional effects of these amino acid substitutions, we first performed *in-vitro* analysis. Initially, Circular Dichroism (CD) spectroscopy was used to confirm that the secondary structure of the mutants was maintained (Figure 3—figure Supplement 1). Then, the K_d of each mutant for EGFR was determined by Isothermal Titration Calorimetry (ITC). ITC measurements of the binding of all mutants to the ECD of EGFR exhibited similar K_d

values to the WT EGF. Only N32R has 2-fold higher affinity for EGFR compared to WT EGF (Figure 3C). All of the EGF mutants displayed a similar secondary structure and interaction with EGFR in-vitro. Thus, the mutations do not appear to affect the receptor through a change in affinity.

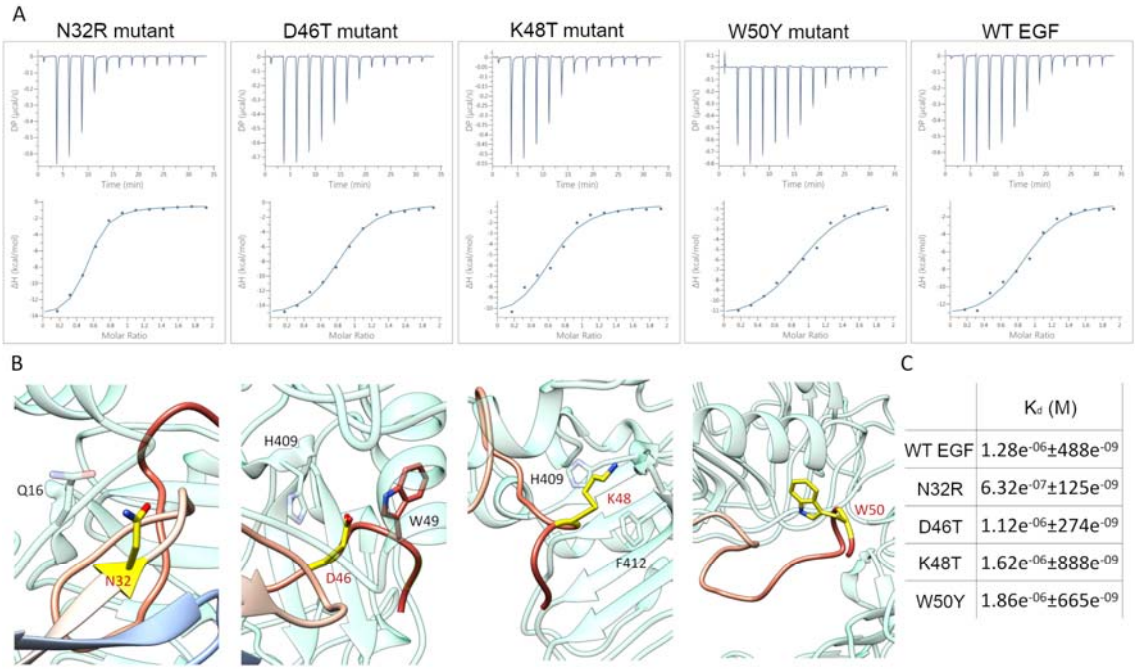

	K_d (M)
WT EGF	$1.28e^{-06}$±$488e^{-09}$
N32R	$6.32e^{-07}$±$125e^{-09}$
D46T	$1.12e^{-06}$±$274e^{-09}$
K48T	$1.62e^{-06}$±$888e^{-09}$
W50Y	$1.86e^{-06}$±$665e^{-09}$

Figure 3. ITC measurements of EGF mutants and the EGFR receptor. (A) ITC analysis of WT EGF ligand and mutants N32R, D46T, K48T, and W50Y binding to the ECD of the EGFR receptor at 25° C. Measurements were taken by adding WT EGF at 200 μM to the ECD of EGFR at 20 μM. **(B)** Four zoom-in of X-Ray structure of the extracellular domain (ECD) of EGFR bound to EGF (PDB 1IVO). In cyan cartoon the ECD of EGFR. Each zoom-in focuses on the mutated residue. Highlighted in yellow stick side chain of the mutated residues and in cyan stick side chain of the residue of ECD in proximity (< 5 Å with the mutated residue. (C) K_d calculated from the ITC measurements using the program Affinimeter KinITC Kintecs Software.

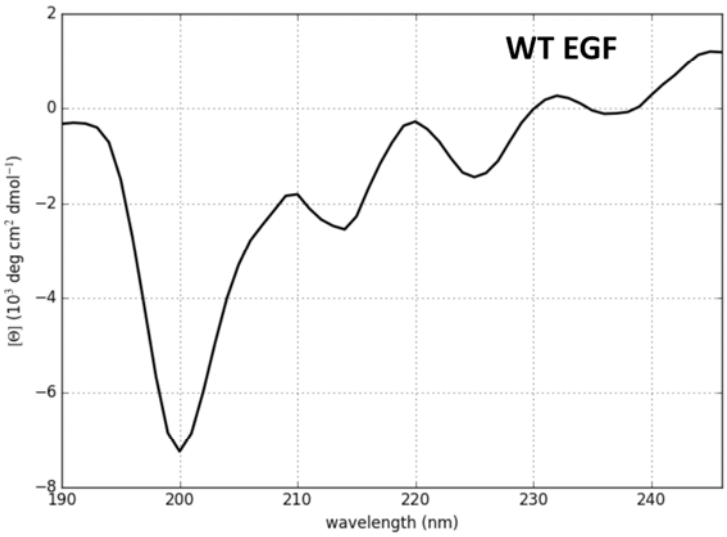

	% β-sheet
WT EGF	0.44
N32R	0.41
D46T	0.47
K48T	0.54
W50Y	0.52

Figure 3—figure Supplement 1. The validation of ordered structure of WT EGF and variants. 0.2 mg/mL of the sample was added to a 10 µm cuvette and analyzed by circular dichroism spectroscopy. All samples showed the presence of a comparable amount of -sheet. The CD spectrum of EGF was similar to previously published results (26). The plot and analysis was made using CAPITO web tool (27).

Biological effects of the EGF mutants

Next, we sampled the effect of the EGF single mutants on EGFR expression and phosphorylation in A431 cells. A431 is a human epidermoid carcinoma cell line that overexpresses EGFR, thus making it easier to observe differences at the receptor level. Treating this cell line with very low (pM) concentrations of EGF has a small effect on proliferation, while high concentration treatments (>10 nM) induces apoptosis (28). We measured the amount of total and phosphorylated EGFR protein at multiple timesteps by Western Blot after treating with saturating concentrations (100 nM) of WT or mutant ligands

(Figure 4). Remarkably, K48T and W50Y showed a greater increase in EGFR phosphorylation 1h after treatment than WT EGF (Figure 4—figure Supplement 1). Treatment with the mutant ligands, but not the WT ligand, also caused a reduction in the amount of EGFR 1h after treatment. At later time points, the effects converge back to the same range of the No Ligand (NL) sample (Figure 4—figure Supplement 2). Thus, while the EGF mutants showed comparable binding affinities to the receptor, at least two of the mutants showed different phosphorylation dynamics compared to the WT ligand. Furthermore, the observed differences in the total amount of EGFR protein indicate a possible alteration in the membrane expression or recycling of the receptor.

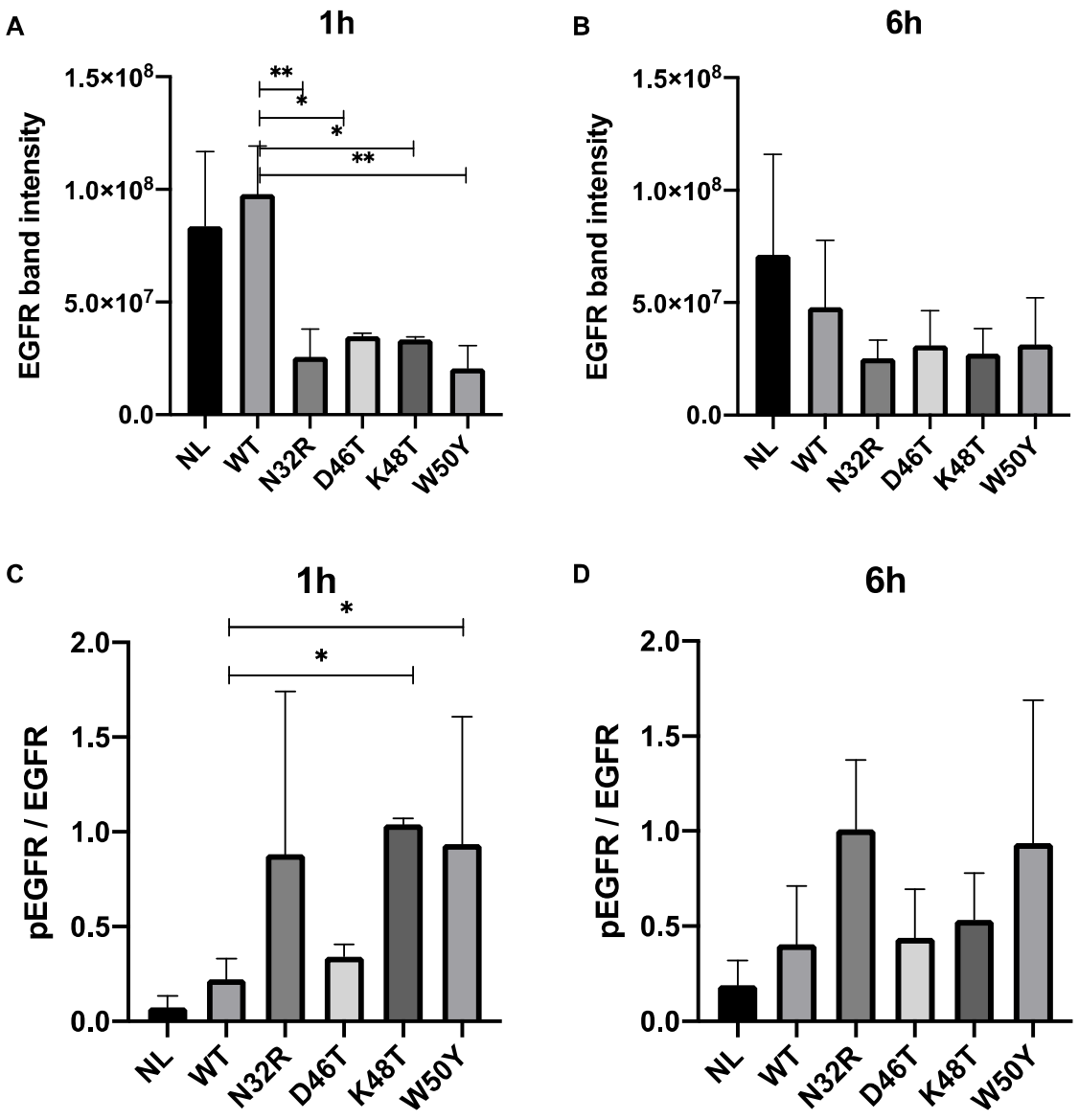

Figure 4. Effects of WT and single-mutant EGF on the receptor in A431 cells. (A-B) Intensity of EGFR band after 1h (A) or 6h (B) treatment of saturating concentrations (100 nM) of the different ligands. (C-D) Relative phosphorylation level, estimated as the ratio of pEGFR (Tyr-1173) band intensity to EGFR band intensity, at 1 h (C) or 6 h (D). All intensities were normalized using the respective alpha-tubulin bands. The bars represent mean ± s.d. (n = 2, technical replicates). Band intensity estimates were calculated using BIO-

RAD ImageLab software (BioRad). Plots and statistics were performed using PRISM software (GraphPad).

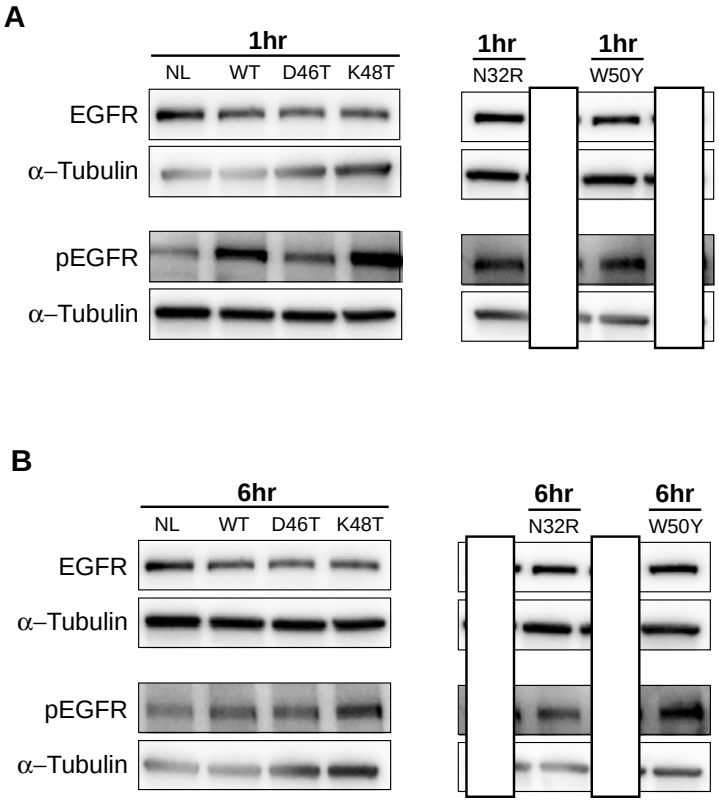

Figure 4—figure Supplement 1. 1h and 6h post-treatment Western Blots. Image of one duplicate of A431 treated cells western blot for 1h (A) and 6h (B). The membrane containing EGFR and tubulin was separated after the transfer. N32R and W50Y gel is the same in both rows, but its lanes have been obscured to facilitate comparison at the same time steps with other samples.

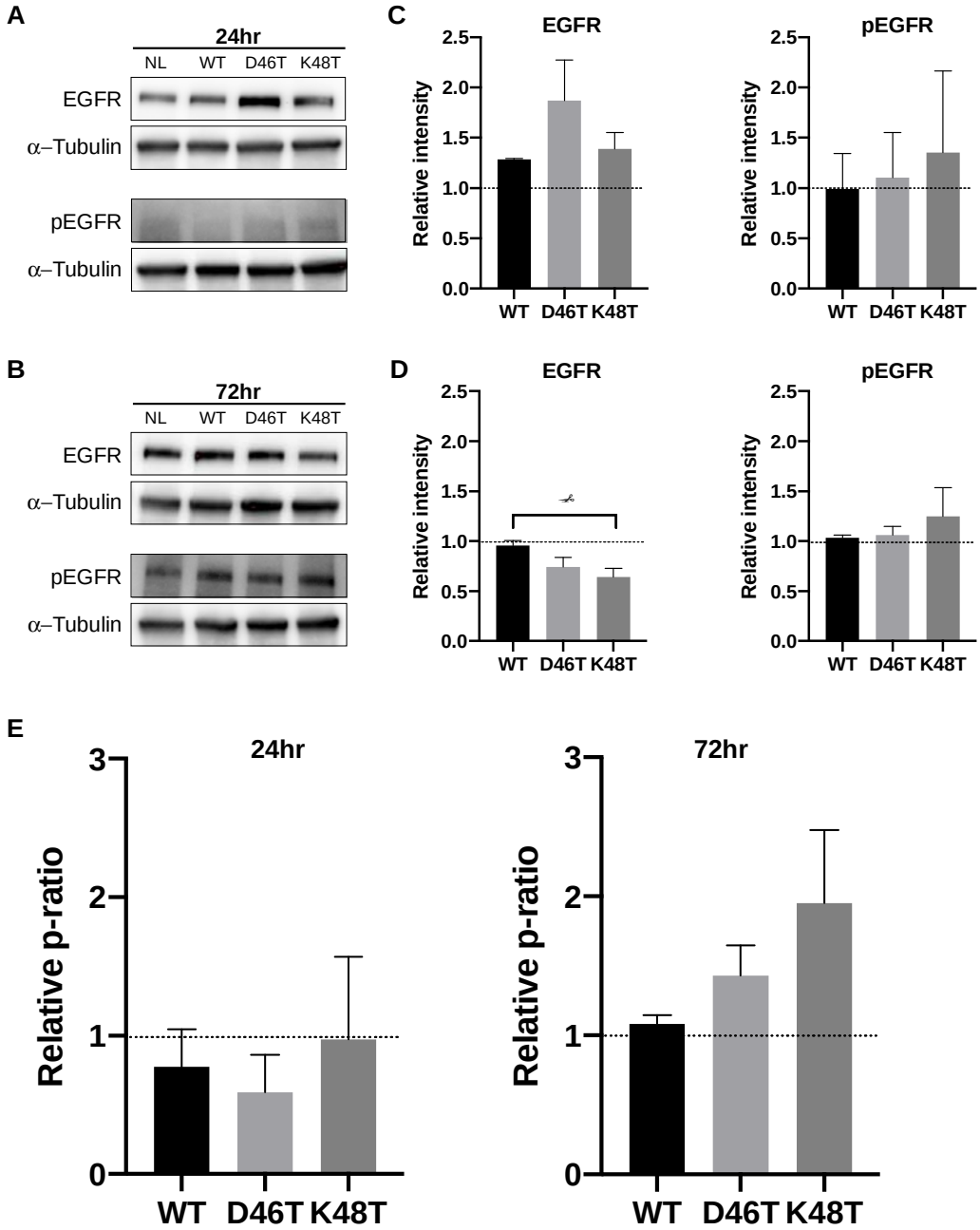

Figure 4—figure Supplement 2. Effects on the receptor at 24h and 72h. (A) Western blot of A431 cells lysate after treatment with No Ligand (NL), WT EGF, D46T or K48T mutants 24h after treatment. (B) Image of the same experiment collected at 72h after treatment. (C) EGFR and pEGFR (Tyr-1173) band intensities, relative to the NL sample at 24h and (D) at 72h after treatment. In (E) and (F), the relative phosphorylation ratio compared to NL respectively at 24h and 72h. A value of 1.0 represent the same phosphorylation ratio as

observed in NL lanes. All intensities were normalized using the respective alpha-tubulin bands. The plots were obtained from duplicate of technical repetitions. Band intensity estimates were calculated using BIO-RAD ImageLab (BioRad). Plots and statistics were performed using PRISM software (GraphPad).

In order to observe the effects of the mutants on the cellular phenotype, we performed a cell growth assay using an IncuCyte® live-cell analysis system. After one day of initial incubation, we subjected Bj5-tα and A431 cells to 1, 10 or 100 nM concentration of growth factors. Treating Bj5-tα fibroblasts with 100 nM WT EGF resulted in a reduction in the proliferation rate compared to the control. The reduction in proliferation was accompanied by a change in cellular morphology that could be a signal of differentiation (Supplementary data 1). However, treatment with any of the mutants decreased the ability of EGF to suppress growth (Figure 5A). The D46T and K48T mutants differed most from the WT (Figure 5—figure Supplement 1). We observed a similar trend in the Albino Swiss mouse 3T3 cell line (Figure 5—figure Supplement 2). In both cell lines, the effects are concentration dependent (Supplementary figure 3). Next, we further tested the mutants in an apoptosis assay using the A431 cell lines. This cell line is known to exhibit apoptosis and reduced growth rate when treated with EGF peptide (29). 48h after treatment with 100 nM WT or mutant EGF, the WT showed the highest decrease in cell proliferation, while the four mutants had an intermediate effect. Cells treated with the W50T mutant had the closest proliferation level to the WT (Figure 5B). In WT EGF cells, we observed evidence of apoptosis in globular processes. Meanwhile, K48T treated cells displayed signs of cellular differentiation (Figure 5C). Significantly, these results show that single amino acid changes in the EGF ligand display differential effects on the EGFR transduction mechanism.

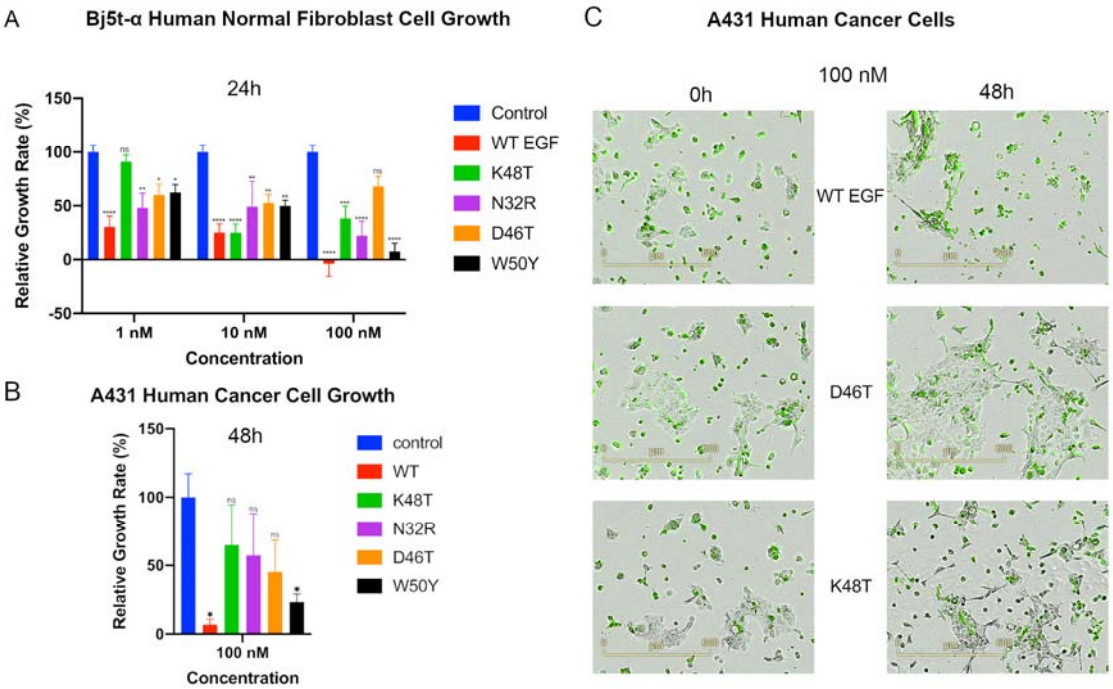

Figure 5. Growth assays of cells treated with EGF variants. (A) Effect of different concentrations of EGF variants on proliferation of the human normal fibroblast Bj5-tα cell line. Data represent the growth rate percentage calculated from the confluence of cells relative to the control (mean ± standard deviation) for each concentration of EGF. Percent confluence was estimated 24 h after the treatment (two replicates per treatment). (B**)** Effect of EGF mutants on the growth of A431 cells. EGF-induced apoptosis is measured as the reduction in cell proliferation compared to the control. (C**)** Comparison of A431 cell growth after treatment with 100 nM WT EGF and EGF variants D46T and K48T. Cells were labeled with fluorescent Annexin V Green Reagent. Plates were pre-warmed prior to data acquisition to avoid condensation and expansion of the plate, which affect autofocus. Images were captured every 2 h (4x magnification) for 3 days in the IncuCyte system.

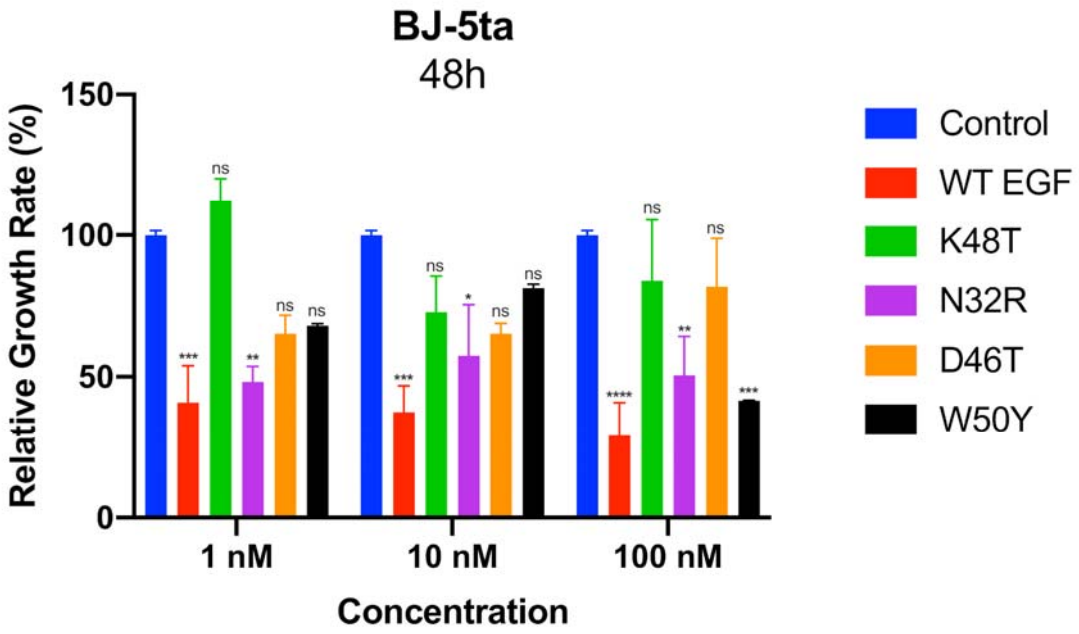

Figure 5—figure Supplement 1. Effect of 1nM, 10nM and 100nM concentrations of EGF variants on the proliferation of the human normal fibroblast Bj5-tα cell line. The data represent growth as a percentage of the control based on the confluence of cells (mean ± standard deviation) for each concentration of EGF. The percentage confluence was estimated 48 h after the treatment (two replicates per treatment).

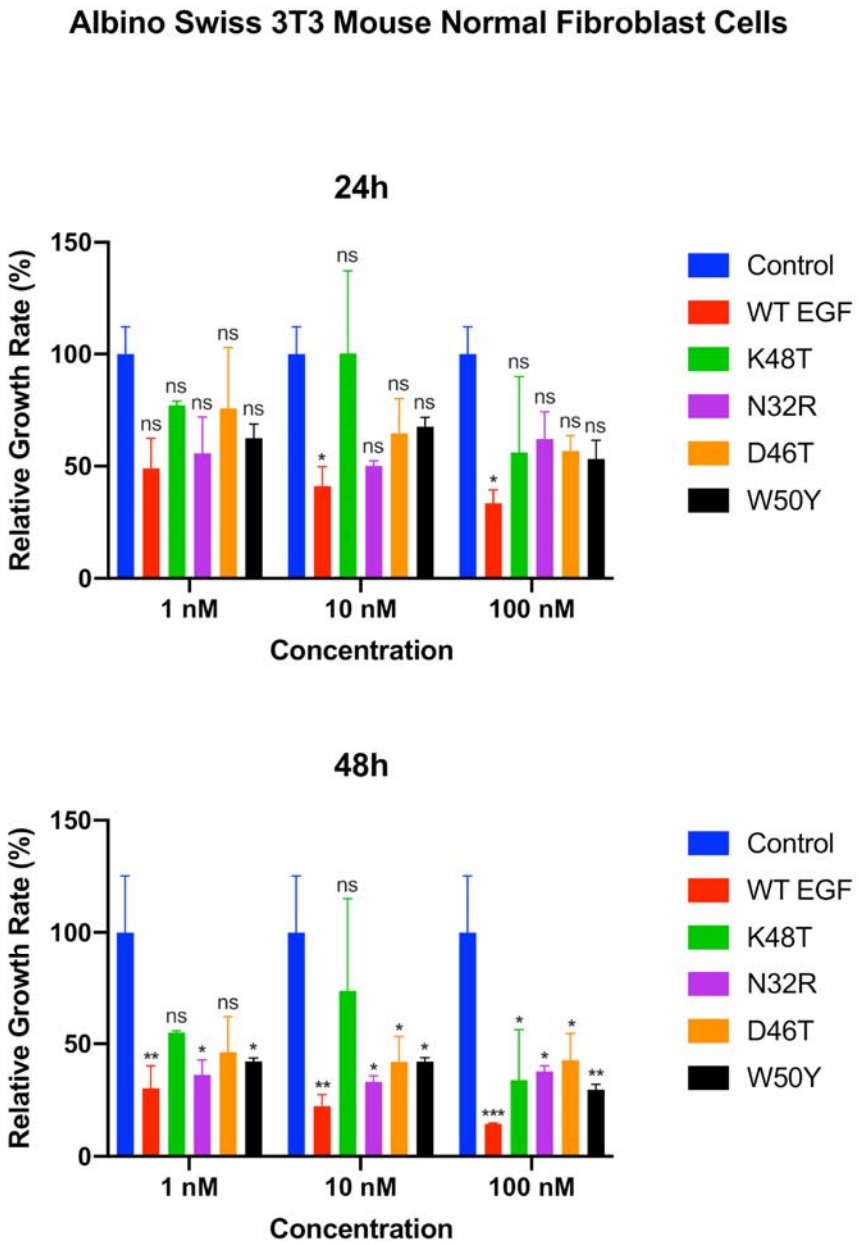

Figure 5—figure Supplement 2. Effect of 1nM, 10nM and 100nM concentrations of EGF variants on the proliferation of the mouse normal fibroblast Albino Swiss 3T3 cell line. The data represent the relative growth percentage to control based on the confluence of cells (mean ± standard deviation) for each concentration of EGF.

Molecular dynamics

To understand how EGF single mutants affect the receptor signaling transduction, we performed full atomistic molecular dynamic (MD) simulations of the extracellular EGFR in complex with WT or mutant ligands (100 ns each). We modeled the receptor starting from the asymmetric, "unstable" conformation of 5WB7 (22). In this way, we expected to observe a fast rearrangement for those simulations where a ligand more favorably induce a stable dimer. In previous literature, an unstable conformation was observed when removing one of the EGF ligands (23). We also performed one simulation of the EGFR dimer in complex with only one WT ligand as a comparison (1ligEGF). The MD simulations quickly converged to a stable RMSD (Figure 6A). For each simulation, we calculated the number of H-bonds between the two receptor dimers, and between ligand and receptor. In the WT EGF simulation, the EGFR dimer had an average of 15 H-bonds, higher than any other simulation (Figure 6—figure Supplement 1A). However, the number of bonds between receptor and ligand was not altered (Figure 6—figure Supplement 1B). In addition, during the course of our simulations we also noted differences in the RMSF specifically located at the dimerization arm domain (Figure 6B). The conformational space sampled by the dimerization arm of K48T simulation was much wider than the WT simulation (Figure 6C). To analyze the temporal distribution of these motion, we measured the distance between Pro-272 and Gly-288 of different EGFR monomers. This distance was chosen because it was able to discriminate between the EGFR dimer in complex with EREG (PDB ID 5WB7) and EGF (PDB ID 1IVO). In 5WB7, one of the two distances is much bigger (~ 1.10 nm vs 0.4 nm) compared to 1IVO (Figure 6—figure Supplement 1C). In our simulations, we observe WT showing a sharp peak at 1 nm, while the mutants and 1ligEGF have a secondary peak at higher distances (Figure 6—figure Supplement 1D). Thus, the mutations in EGF appear to

affect the stability of the EGFR dimer without affecting the stability of the EGF-EGFR interaction.

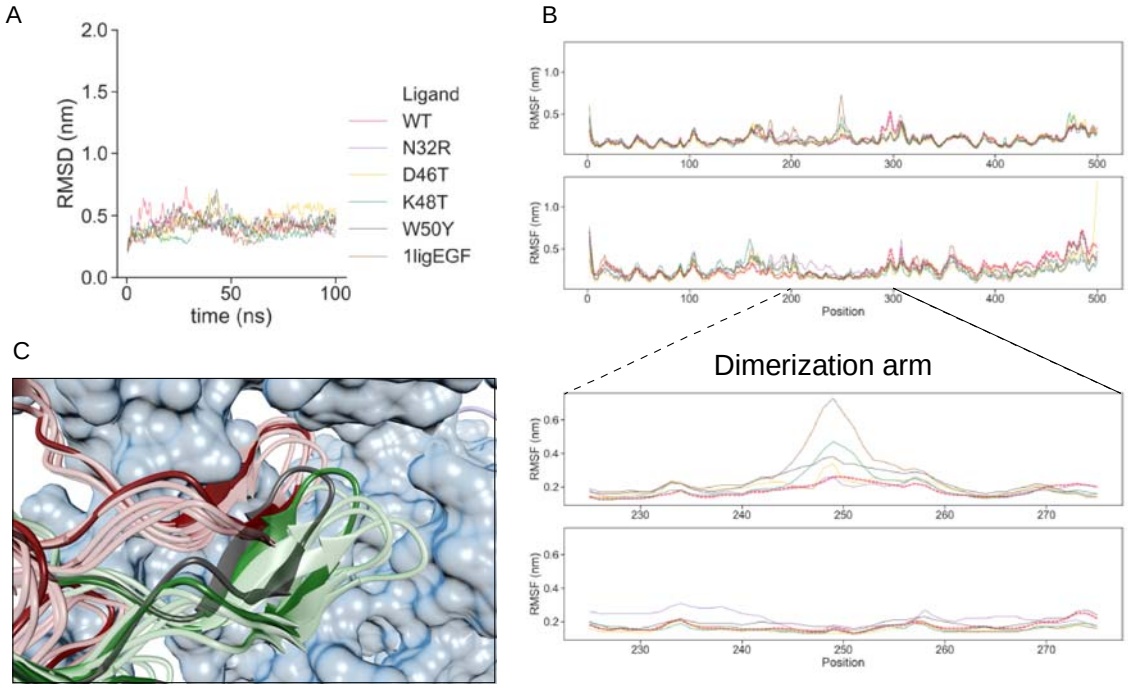

Figure 6. Molecular Dynamics of the EGFR extracellular domain. (A) Root Mean Square Deviation from the initial structure. (B) Top, Root Mean Square Fluctuations of the 100 ns simulations. The WT level is marked in bold and dashed red line. Bottom, focus on the RMSF of the dimerization arm domain. The two plots represent the two EGFR in the receptor dimer. (C) Dynamics of the dimerization arm domain in WT (red) and K48T (green) simulations. A structure every 20 ns of simulation was taken and aligned to 1IVO reference structure (blue surface and black ribbon). The structure at 20 ns is represented in solid colors. K48T simulation shows a more dynamic dimerization arm.

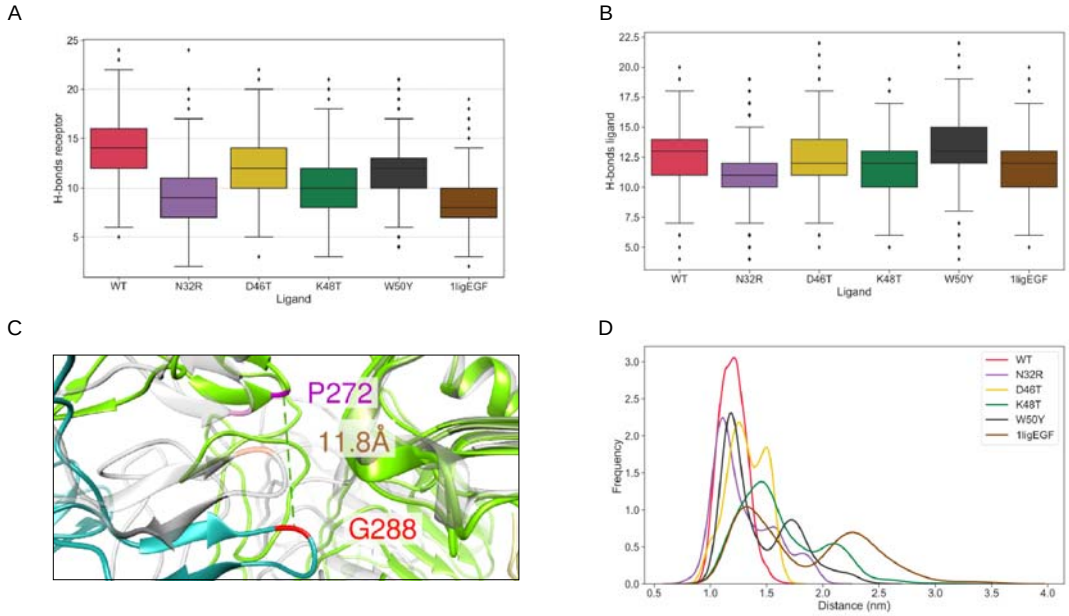

Figure 6—figure Supplement 1. RMSF and distance between Pro-272 and Gly-288. (A) Number of H-bonds formed between the two receptors during the 100 ns simulation time. (B) Number of H-bonds formed between the receptor that shows a dynamic dimerization arm and the corresponding ligand during the 100 ns simulation time. (C) Distance used to investigate the fluctuations of the dimerization domain highlighted on the structure. Pro 272 (purple) and Gly 288 (red) are highlighted both on 5WB7 (green and teal) and in 1IVO (grey). The distance between the alpha carbons of the 5WB7 couple is shown in brown and is notably longer than 1IVO. (D) Distribution of the distance between Pro272 and Gly 288 in all the simulations. WT simulation shows a single peak at ~1nm, while in all other ligands the distance has two peaks.

Discussion

The prediction of functional residues is a well-developed field (30), where conservation measures are considered a key factor to rely on. Tools such as ConSurf (31) and the ET-like methods (32) are able to identify slowly evolving positions that are involved in folding, interaction, or catalytic activity (30). However, the specific reason why a residue is conserved

often remains unclear. In this work, we show a new method to identify residues that affects specific functions in a system of interest. Our approach combines a conservation score calculated from the structural alignment of paralogs and among orthologs, with an intra- and inter-molecular co-evolution score with previously known interactors. Conservation and coevolution give a complementary signal, thus improving the overall predictive performance (33). The coevolution score was introduced to DIRpred to highlight residues that are directly responsible of an interaction with the receptor, at the expenses of those that interact intramolecularly within the ligand. While the first part efficiently identifies Asn-32 and Lys-48 as putative interactors, the second part does not properly give a penalty to residue Tyr-29. The interaction of this position with His-10 is also conserved in EGF but with reversed positioning (Figure 2 – figure supplement 3), resulting in a low paralog conservation (then high contribution to DIRpred score). While it is still possible to optimize the co-evolution scoring function, integrating conservation and coevolution measures is a promising way to recall information of specific functions involving protein-protein interactions.

Three out of the four positions were highlighted by previous reports, however none of them were individually mutated. The tryptophan in position 50 is a strong outlier in our bioinformatics analysis, along with Trp-49 (Figure 2). Their score is high even when using conservation measures that do not take amino acid type change into account (data not shown). However, Trp-50 was a better candidate for testing because of its outward facing position, and since Trp-49 is involved in buried protein contacts (34). Trp-49 and Trp-50 could be responsible in facilitating the interaction of EGF with the membrane phospholipids, as it happens for Pro-7 and Leu-8 (35). In 1992, a biophysics work showed how Trp-49 and Trp-50 are not burying inside the bilayer when EGF and a membrane are in solution alone (36), though this might be different when in complex with the receptor. For example, this could be

achieved by Trp-50 through the formation of a helix, clustering together with Val-34 and Arg-45 around the conserved Leu-47 (37). Mutation N32R is on the interface between ligand and receptor. The slightly higher affinity is probably due to the presence of the guanidinium group of R which is positively charged and could interact with Gln-16 of EGFR ECD (Supplementary figure 2). Interestingly, mutations of the corresponding position in chicken TGFA were able to alter the mitogenicity without strongly affecting the binding affinity (38). While no previous literature reported about Asp-46 before, Lys-48 was found in two mutants that showed higher affinity (39). Our results give an explanation of the previous reports, while shedding new light on the role of the previously unreported Asp-46.

With the exception of N32R, all mutant ligands do not change in binding affinity to EGFR of compared to the wild type ligand. However, the mutants showed a different cellular effect on Bj-5ta cells (Figure 5). A delayed proliferation response compared to control might seem counterintuitive for fibroblast (40). Though, Bj-5ta hTERT immortalized fibroblasts show features that distinguish them from *in vivo* fibroblast, like differential gene expression and epiregulin-dependent proliferation (41). A decrease in cell proliferation after EGF treatment could be the result of competition between the endogenously synthesized epiregulin and EGF, thus altering the balance between proliferation and differentiation.

A431 cells constitutionally express EGFR at high levels. Treatment with EGF has been observed to promote STAT1 dependent apoptosis (42). This pathway is dependent on the internalization of the ligand-receptor complex by the endocytosis process, a key factor in the ligand-induced biased signaling (17). In our experiments, A431 cells treated with mutant EGF ligands show a higher growth rate, therefore a decreased rate of apoptosis compared to WT. Given the setting of the experiment, modularity in the endocytosis pathway is a straightforward explanation to the observed differences in growth rate and in protein levels

and phosphorylation. Interestingly, K48T treated cells showed an increase in long and thin cellular processes in all replicates (Figure 5). This mutant was also observed with a markedly higher EGFR phosphorylation 1 h after treatment (Figure 3). A possible explanation could be EGF-induced tubular formation, an alternative EGF-induced pathway reported in intestinal epithelial cells (43). In both the cellular growth experiments, the growth rate of the mutants is intermediate between the control and EGF, and concentration dependent. This phenomenon, and the cell-line specific response of growth hormones is consistent with previous literature reports (44).

The observation that the four mutations in EGF alter signal transduction without disrupting any contacts between the ligand and the receptor can be explained by the “loss of symmetry” model of EGFR signaling (19). Freed *et al.* observed how stable symmetrical dimers show a short-lived nature of signaling, while asymmetric dimers conduct a sustained activation, lasting longer than 24 h. Such a model provides an explanation on how a low level of phosphorylation after EGF treatment causes the apoptotic behavior observed in the cellular growth experiments. Compared with WT EGF, the K48T and W50Y variants show a higher phosphorylation signal, suggesting a more sustained activation of EGFR, possibly through the formation of a less stable, asymmetric dimer. Thus, the observed effects of the EGF mutations on EGFR phosphorylation and dimer stability are consistent with the "loss of symmetry" mechanism.

The analysis of the fluctuations in the dimerization arm reveals an underlying bias in ligand-induced receptor dimerization, originally not visible from the static images of structure comparison. K48T is the mutant that induce the biggest deviation from the WT, in accordance to the phosphorylation data. Although, all mutants show a transition. While

giving an initial outlook on the effect of the mutants, our MD simulations do not take into account other factors that could be important in the mechanism of action of EGFR. Differential multimerization (45), receptor glycosylation, and the interaction with the membrane (23) are factors where the underlying bias induced by the mutant ligands could also have an effect in.

In this work, we showed how a single mutation of EGF is able to alter the specific functional relationship with the receptor. For functional divergence to arise, it could take as little as mutating 15% of the sequence (47). However, the EGFR ligands divergence date back to the vertebrate ancestor of R1/R2 whole genome duplication, up to 500 million years ago (48), as hinted by the low (~25%) sequence identity. From our results, the sequence distance does not reflect the distance in function. In fact, the functional divergence of EGF was altered with just a single targeted mutation.

In conclusion our data suggests that a single mutant ligand induces a conformational change of the receptor that then affects receptor dimer stability, with plausible effects on phosphorylation level and downstream pathway activation (49). This shows how the persistence of biased signaling in EGFR is in an unstable equilibrium, where the observed conservation of diverging sites among paralogs is naturally reinforced to maintain the functional divergence. To determine whether a short distance in function space among paralogs is a consequence or a necessity for living systems, further studies will be required.

Materials and Methods

Sequence and structure analysis

The sequences of EGFR ligands and the multiple sequence alignment of EGF orthologs were obtained from the Ensembl database (51). Multiple sequence alignment (MSA) of all ligands was performed with MAFFT software (52). X-ray structures were obtained from the PDB database (53). Structural alignments were created using Chimera (54).

Phylogenetic analysis

From the multiple sequence alignment of EGF from different species, nearly identical sequences were removed. The *Drosophila melanogaster* EGF sequence was added as an outgroup in the EGF phylogeny, while *Caenorhabditis elegans* EGF was used as outgroup for the ligand phylogeny. MSA and phylogenetic tree images were created using Unipro UGENE software (55). Three phylogenetic trees were made using the Neighbor Joining (NJ), Maximum Likelihood (ML), and Bayesian (MrB) methods in IQTREE (56), using ModelFinder to scan for the best-fit evolutionary model and parameters (57).

Divergence Inducing Residue PREDiction

We identified sites in EGF responsible for functional divergence using a method that combines evolutionary and co-evolutionary data, called DIRpred (Divergence Inducing Residue PREDiction). The DIRpred scoring function combines four components to evaluate each residue: I) The combined conservation scores in the ortholog alignments. This score is calculated by averaging the conservation of a reference ligand site with the conservation in the respective positions of the other ligands' orthologs alignments; II) The complementary value (1 – x) of the conservation score in the paralogs alignment. This score can be obtained either from sequence alignment (paralogs MSA) or structural alignment (paralogs MSTA). III) The highest co-evolution score between a reference ligand site and all of the receptor sites. IV) The complementary value (1 – x) of the highest co-evolution score between a

reference ligand site and all of the other ligand sites in the joint orthologs alignment of all ligands (Figure 7).

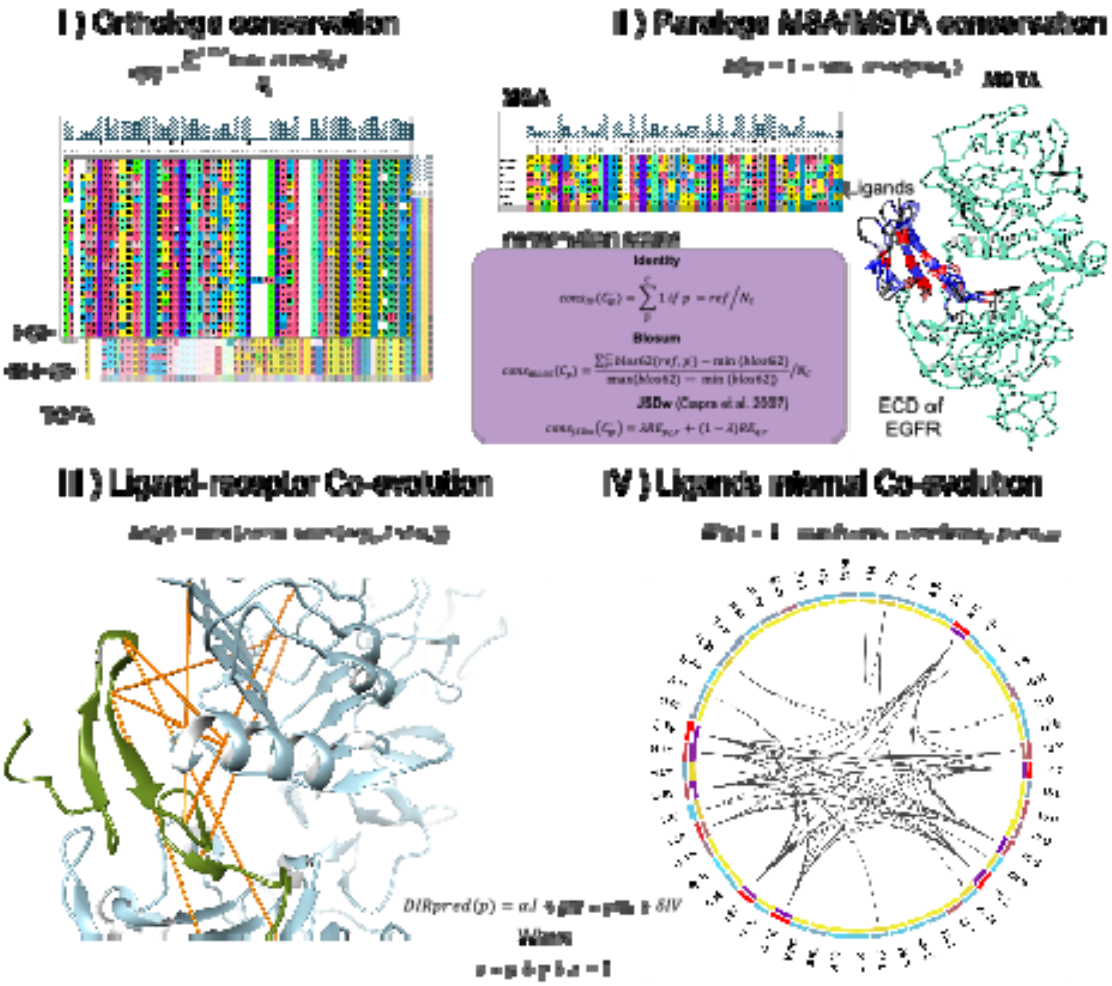

Figure 7. DIRpred rationale. The prediction of Divergence Inducing Residues consists of a linear combination of four site-specific scores, in roman numerals. In I, the orthologs MSA of each paralog is used to compute a conservation score (as exemplified from the histograms on the alignments). Alignment images were produced using Unipro software (58). In II, the human paralog sequences or structures were aligned and the same conservation score function was used. In the purple box, the conservation score functions are represented. In III, the co-evolution score between EGF and each receptor site was computed using Mutual Information (MI). The yellow lines on the structure connect the highest scoring co-evolving

residues between ligand and receptor. In IV, MI co-evolution score was computed from the combined ligands orthologs alignment. The circular plot was performed using MISTIC2 (59).

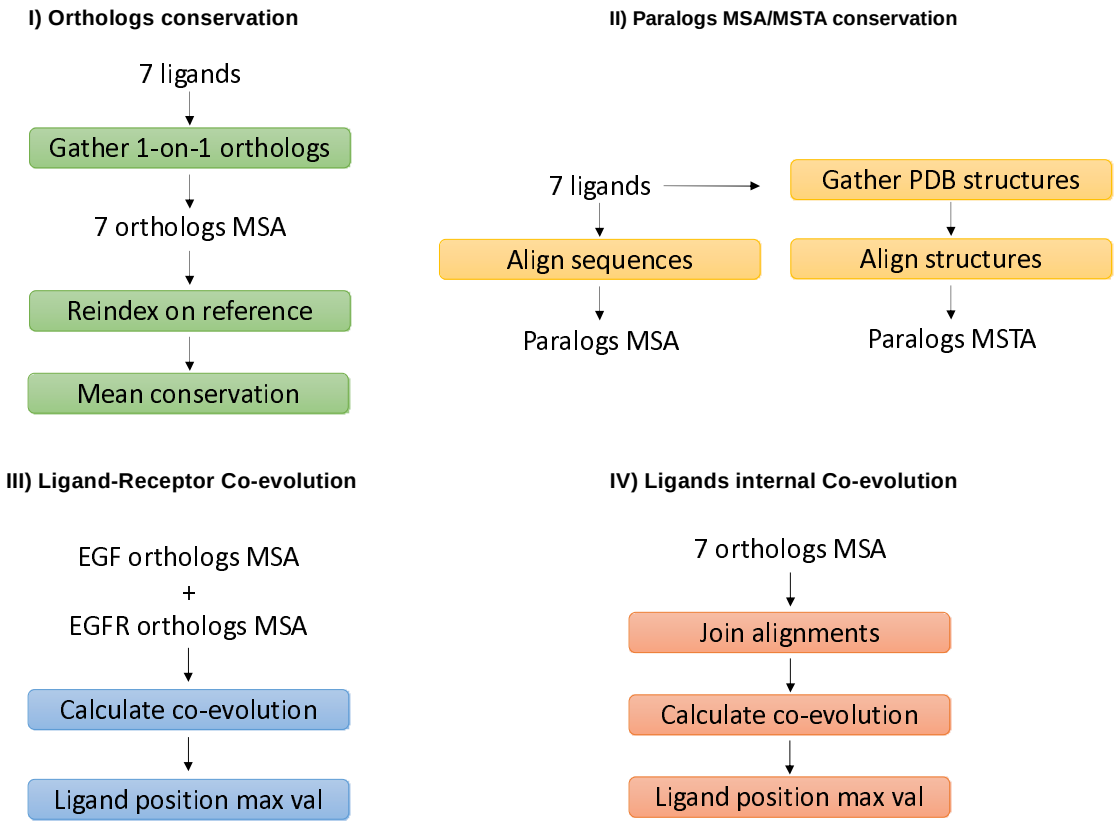

Figure 7—figure Supplement 1. DIRpred schema. A schematic representation of the previous figure, showing the workflow to produce each of the four scores.

Conservation scores were calculated using three different formulations: 1) IDENTITY, 2) BLOSUM, and 3) JSDw. The IDENTITY score measures the frequency of appearance of a reference residue in the MSA. The BLOSUM score takes the amino acid substitution frequency into account using the BLOSUM62 matrix, normalized by the maximum and minimum score for the BLOSUM matrix. The JSDw score is based on Jensen Shannon divergence with a window of residues (60). The analysis and plots were performed with

Python3 package SEABORN. EGF index positions from the paralogs MSA and MSTA were respectively used to align the MSA and MSTA based scores.

The code used in the analysis of the DIRpred score and plots and the data used in this paper are shared on Github: https://github.com/oist/DIRpred.

Selection of the mutations

Along with the DIRpred score, the choice of positions for mutation was influenced by two manually curated factors: the distance from the receptor and the amino acid variation among ligand types. We designed mutations with the aim of inferring a transition to the amino acid properties in sites where the ligands show a different pattern. Overlapping residues at a given position were divided into two groups, based on an EGF-like and non EGF-like stabilization of the receptor dimer. This property was previously shown to follow binding affinity (19). Residues that introduced a noticeable shift in amino acid properties between the two groups were selected. For example, position N32 is hydrophobic in the high affinity ligands group, positively charged in the low affinity group and negatively charged in EGF. Finally, we carefully analyzed exceptional cases in the DIRpred scoring. Some of the residues that show high score have intramolecular interactions with another amino acid in the ligand. These residues, if mutated, will lose EGF structural stability (namely "residue swapping" behavior showed in Figure 2—figure Supplement 3**)**. The decision of which mutation to introduce was made using the paralogs alignment. Positions 32, 48 and 50 have high DIRpred score. Position 46 was included although having a lower score, because the substitution pattern matches the two ligands groupings. Furthermore position 46, 48 and 50 were preferred because, given previous experiments and the overall scores, the EGF C-terminus tail seems to play a critical role in the ligand function, for example (61).

Synthetic Peptides

The wild-type, N32R, D46T, K48T, and W50Y variants of EGF were ordered from Scrum Net Co with purity >90% and quantity 5 mg/mL. These peptides were used for ITC measurements, Circular Dichroism (CD) measurements, proliferation studies, and Western Blot (WB) analyses.

Cell Lines

The *Bj5-tα human normal fibroblast cell line* was purchased from ATCC. Cells were grown in DMEM with 10% fetal bovine serum (FBS), and 5 µg/mL hygromycin B. The *Swiss Albino 3T3* mouse *normal fibroblast cell line* was obtained from the RIKEN Cell Bank. Cells were grown in DMEM, 10% FBS, 50 ug/mL gentamycin at 37°C in a 5% CO_2 atmosphere with 95% humidity. The *A431 human epithelial carcinoma adherent cell line* (RIKEN Cell Bank) is a model skin cancer cell line with overexpressed EGFR used for oncogenic pathway studies (62).Cells were cultured in DMEM supplemented with 10% FBS (Sigma-Aldrich), 50 ug/mL gentamycin antibiotic or a combination of 100 unit/ml Penicillin G (Nacalai Tesque) and 100 µg/ml streptomycin sulfate (Nacalai Tesque). Experiments were conducted at 37°C in a 5% CO_2-enriched air atmosphere with 95% humidity. Cell lines were grown and used for Western Blot and cell proliferation studies.

Cell Proliferation Assay

We measured cell proliferation using a label-free, non-invasive, cellular confluence assay with IncuCyte Live-Cell Imaging Systems (Essen Bioscience). Human Bj5-tα (2,500 cells / well) and Mouse Swiss Albino 3T3 (1,000 cells/well) were seeded overnight on a 96-well plate (Corning) at 37°C in an incubator. The next day, cells were treated with WT EGF and mutants at 1 nM, 10 nM and 100 nM concentrations and placed in an XL-3 incubation

chamber maintained at 37°C. The plate was scanned using a 4x objective at 2-hr intervals over 3 days. Cell confluence was measured using IncuCyte Analysis Software. The IncuCyte Analyzer gives real-time confluence data based on segmentation of high-definition phase-contrast images. Cell proliferation is shown as an increase in confluence rate relative to control.

Apoptosis Assay

Experiments were performed with the A431 human cancer cell line. 5,000 cells/well were seeded on a 96-well plate (Corning) and incubated at 37°C for 24 hr. Media were replaced with fresh DMEM containing WT EGF, or EGF mutants at 1, 10, and 100 nM concentrations and fluorescent annexin V green reagent. Plates were pre-warmed prior to data acquisition to avoid condensation and expansion of the plate, which affect autofocus. Images were captured every 2 hrs (4x) for 3 days in the IncuCyte system. Cell proliferation is reported as in the previous assay.

Statistics

Proliferation and apoptosis experiments were performed in duplicates. All results are shown as the mean±s.d. Raw data was analyzed by two-way ANOVA with 95% confidence level. The multiple test was corrected using Bonferroni post hoc test. Prism 8 software was used for statistical analysis. Asterisks in the pictures show P-values using GraphPad convention: 0.1234 > (ns), 0.0332 > (*), 0.0021 > (**), 0.0002 > (***), 0.0001 > (****).

Isothermal Titration Calorimetry (ITC)

All ITC studies employed a MicroCal PEAQ-ITC System (Malvern). For titration, both EGFR ECD (Sigma-Aldrich) and EGF variants were dialyzed into the same reaction buffer

Milli-Q H_2O (22 μm) at 25°C. Each titration involved serial injections of 13 × 3 μL aliquots of EGF variants (200 μM) into a solution of EGFR ECD (20 μM) in the sample cell. In each case, the reference cell was filled with the same reaction buffer as the control to determine the heat upon binding of the two components. The measured heat constant value was subtracted from the heat per injection prior to analysis of the data. The experiment was replicated twice. Results were analyzed by MicroCal PEAQ-ITC Analysis Software.

Circular Dichroism (CD)

Far UV measurements were taken at a protein concentration of 0.1 μM, using a cuvette with a path length of 0.1 cm. Secondary structure content was calculated from far UV spectra using CAPITO software (27). Five scans in the 190-240-nm wavelength range were taken.

Western Blot Analysis

A431 epidermoid carcinoma cells were harvested using Lysis Buffer (0.4% SDS, 1 mM DTT, 1%). Samples were incubated at 37°C for 10 min with Benzonase and centrifuged at 15,000 rpm at 22°C for 10 min. Supernatants were used for further analysis. Sample concentrations were measured with a BCA protein assay kit (ThermoFisher Scientific). Lysate were mixed with 4x Sample Loading Laemmli Buffer and incubated at 90°C for 5 min. Equal amounts of protein were loaded in 12% Mini PROTEAN® TGX™ SDS-PAGE gel (Bio-Rad) and transferred to PVDF membranes (Trans-Blot Turbo RTA Mini 0.2 μm PVDF Transfer Kit). Membranes were blocked for 10 min with Bullet Blocking One (Nacalai) and reacted with monoclonal rabbit anti-EGFR antibody (Cell Signaling Technology, Inc.), Phospho-EGF Receptor (Tyr1173) (Cell Signaling Technology, Inc.), monoclonal rabbit anti-PLCy (Cell Signaling Technology, Inc.), and anti-phosphorylated PLCy antibodies (Cell Signaling Technology, Inc.), rabbit anti-PKCζ (Cell Signaling Technology, Inc.), rabbit anti-phospho-

PKCζ/λ (Thr410/403) (Cell Signaling Technology, Inc.) and rabbit anti-α-tubulin pAb (MBL) at dilution of 1:1000. Samples were incubated with Goat Anti-Rabbit IgG HRP at a 1:5000 dilution and chemiluminescent signals were detected by CDP Plus (ThermoFisher Scientific) and ChemiDoc touch MP (Bio-rad).

Molecular Dynamics

All the simulations were performed with Gromacs version 2020 (63) using charmm36-mar2019 force field (64) and SPC216 for water. PDB ID 5wb7 was used as model and template. EGF structure model was extracted from PDB ID 1ivo and superimposed to the ligand using UCSF Chimera Match-Maker algorithm (65). Mutants were generated using Swissmodel webserver (66), while missing atoms were compensated using Scwrl4 (67). A system was composed of EGFR dimer in complex with one or two EGF wild type (WT), N32R, D46T, K48T or W50Y were solvated and neutralized using NaCl ions in a dodecahedral box. Then, energy temperature and pressure equilibrations were performed to the system following the guidelines in Lemkul 2019 (68).

A 100 ns production simulation was run using the Verlet cut-off scheme (69) for non-bonded interactions and LINCS as constraint algorithm (70). All the simulations reached convergence of RMSD. Long range electrostatic interactions were computed using the Particle Mesh Ewald method (71) using a dedicated GPU. The parameter files for all runs are included in the supplementary data [#ADD#]. We checked for differences in relative motions between the three simulations by extracting and concatenating the backbone trajectories using catDCD plugin of VMD (72), then performing a PCA using Bio3d R package (73).

Author contributions

PL, SP, DM conceived and designed the project; SP developed and performed the computational models and analyses; DM and GU performed the experiments; all authors analyzed the data and wrote the manuscript.

Acknowledgments

We thank Tadashi Yamamoto, Ichiro Maruyama for providing the antibodies, Keiko Kono for the technical help with the WB experiments. We are grateful for the help and support provided by the Scientific Computing section of Research Support Division and in particular Jan Moren at OIST. We thank Madhuri Gade, Mirco Dindo, Harry Wilson and Benjamin Clifton for critical reading. We thank Pierre Matricon for the discussion on the molecular dynamics data, Russel Alenton on the cell proliferation assay and Christine Guzman on the western blot analyses.

Funding

Financial support by the Okinawa Institute of Science and Technology to P.L. is gratefully acknowledged.

References

1. Gazdar AF. Activating and resistance mutations of EGFR in non-small-cell lung cancer: role in clinical response to EGFR tyrosine kinase inhibitors. Oncogene. 2009;28:S24-S31.
2. Oda K, Matsuoka Y, Funahashi A, Kitano H. A comprehensive pathway map of epidermal growth factor receptor signaling. Mol Syst Biol. 2005;1:2005.0010.
3. Landau M, Fleishman SJ, Ben-Tal N. A putative mechanism for downregulation of the catalytic activity of the EGF receptor via direct contact between its kinase and C-terminal domains. Structure. 2004;12(12):2265-75.
4. Purba ER, Saita EI, Maruyama IN. Activation of the EGF Receptor by Ligand Binding and Oncogenic Mutations: The "Rotation Model". Cells. 2017;6(2).
5. Wilson KJ, Gilmore JL, Foley J, Lemmon MA, Riese DJ, 2nd. Functional selectivity of EGF family peptide growth factors: implications for cancer. Pharmacol Ther. 2009;122(1):1-8.

6. Nicholson RI, Gee JM, Harper ME. EGFR and cancer prognosis. European journal of cancer (Oxford, England : 1990). 2001;37 Suppl 4:S9-15.
7. Xu MJ, Johnson DE, Grandis JR. EGFR-targeted therapies in the post-genomic era. Cancer Metastasis Rev. 2017;36(3):463-73.
8. Alvarez-Ponce D, Feyertag F, Chakraborty S. Position Matters: Network Centrality Considerably Impacts Rates of Protein Evolution in the Human Protein-Protein Interaction Network. Genome Biol Evol. 2017;9(6):1742-56.
9. Jensen RA. Orthologs and paralogs - we need to get it right. Genome Biol. 2001;2(8):Interactions1002.
10. Rao VS, Srinivas K, Sujini GN, Kumar GN. Protein-protein interaction detection: methods and analysis. International journal of proteomics. 2014;2014:147648.
11. Groenen LC, Nice EC, Burgess AW. STRUCTURE-FUNCTION-RELATIONSHIPS FOR THE EGF/TGF-ALPHA FAMILY OF MITOGENS. Growth Factors. 1994;11(4):235-57.
12. Souriau C, Gracy J, Chiche L, Weill M. Direct selection of EGF mutants displayed on filamentous phage using cells overexpressing EGF receptor. Biol Chem. 1999;380(4):451-8.
13. Skwark MJ, Raimondi D, Michel M, Elofsson A. Improved Contact Predictions Using the Recognition of Protein Like Contact Patterns. PLOS Computational Biology. 2014;10(11):e1003889.
14. Gocheva G, Ivanova A. A Look at Receptor-Ligand Pairs for Active-Targeting Drug Delivery from Crystallographic and Molecular Dynamics Perspectives. Mol Pharm. 2019;16(8):3293-321.
15. Evans BA, Sato M, Sarwar M, Hutchinson DS, Summers RJ. Ligand-directed signalling at beta-adrenoceptors. Br J Pharmacol. 2010;159(5):1022-38.
16. Kenakin T. Functional selectivity and biased receptor signaling. J Pharmacol Exp Ther. 2011;336(2):296-302.
17. Ali R, Brown W, Purdy SC, Davisson VJ, Wendt MK. Biased signaling downstream of epidermal growth factor receptor regulates proliferative versus apoptotic response to ligand. Cell Death Dis. 2018;9(10):976.
18. Strachan L, Murison JG, Prestidge RL, Sleeman MA, Watson JD, Kumble KD. Cloning and biological activity of epigen, a novel member of the epidermal growth factor superfamily. The Journal of biological chemistry. 2001;276(21):18265-71.
19. Freed DM, Bessman NJ, Kiyatkin A, Salazar-Cavazos E, Byrne PO, Moore JO, et al. EGFR Ligands Differentially Stabilize Receptor Dimers to Specify Signaling Kinetics. Cell. 2017;171(3):683-95.e18.
20. Mehrabi M, Mahdiuni H, Rasouli H, Mansouri K, Shahlaei M, Khodarahmi R. Comparative experimental/theoretical studies on the EGFR dimerization under the effect of EGF/EGF analogues binding: Highlighting the importance of EGF/EGFR interactions at site III interface. Int J Biol Macromol. 2018;115:401-17.
21. Knudsen SL, Mac AS, Henriksen L, van Deurs B, Grovdal LM. EGFR signaling patterns are regulated by its different ligands. Growth Factors. 2014;32(5):155-63.
22. Liu P, Cleveland TEt, Bouyain S, Byrne PO, Longo PA, Leahy DJ. A single ligand is sufficient to activate EGFR dimers. Proc Natl Acad Sci U S A. 2012;109(27):10861-6.
23. Arkhipov A, Shan Y, Kim ET, Shaw DE. Membrane interaction of bound ligands contributes to the negative binding cooperativity of the EGF receptor. PLoS Comput Biol. 2014;10(7):e1003742.
24. Chagoyen M, García-Martín JA, Pazos F. Practical analysis of specificity-determining residues in protein families. Briefings in Bioinformatics. 2015;17(2):255-61.

25. Cochran JR, Kim YS, Lippow SM, Rao B, Wittrup KD. Improved mutants from directed evolution are biased to orthologous substitutions. Protein Eng Des Sel. 2006;19(6):245-53.
26. Prestrelski SJ, Arakawa T, Wu CS, O'Neal KD, Westcott KR, Narhi LO. Solution structure and dynamics of epidermal growth factor and transforming growth factor alpha. The Journal of biological chemistry. 1992;267(1):319-22.
27. Wiedemann C, Bellstedt P, Gorlach M. CAPITO--a web server-based analysis and plotting tool for circular dichroism data. Bioinformatics. 2013;29(14):1750-7.
28. Gill GN, Lazar CS. Increased phosphotyrosine content and inhibition of proliferation in EGF-treated A431 cells. Nature. 1981;293(5830):305-7.
29. Gulli LF, Palmer KC, Chen YQ, Reddy KB. Epidermal growth factor-induced apoptosis in A431 cells can be reversed by reducing the tyrosine kinase activity. Cell Growth Differ. 1996;7(2):173-8.
30. Nemoto W, Saito A, Oikawa H. Recent advances in functional region prediction by using structural and evolutionary information - Remaining problems and future extensions. Computational and structural biotechnology journal. 2013;8:e201308007.
31. Ashkenazy H, Abadi S, Martz E, Chay O, Mayrose I, Pupko T, et al. ConSurf 2016: an improved methodology to estimate and visualize evolutionary conservation in macromolecules. Nucleic Acids Res. 2016;44(W1):W344-W50.
32. Lichtarge O, Bourne HR, Cohen FE. An evolutionary trace method defines binding surfaces common to protein families. J Mol Biol. 1996;257(2):342-58.
33. Teppa E, Wilkins AD, Nielsen M, Buslje CM. Disentangling evolutionary signals: conservation, specificity determining positions and coevolution. Implication for catalytic residue prediction. BMC Bioinformatics. 2012;13(1):235.
34. Gallay J, Vincent M, Li de la Sierra IM, Alvarez J, Ubieta R, Madrazo J, et al. Protein flexibility and aggregation state of human epidermal growth factor. A time-resolved fluorescence study of the native protein and engineered single-tryptophan mutants. Eur J Biochem. 1993;211(1-2):213-9.
35. Tynan CJ, Roberts SK, Rolfe DJ, Clarke DT, Loeffler HH, Kastner J, et al. Human epidermal growth factor receptor (EGFR) aligned on the plasma membrane adopts key features of Drosophila EGFR asymmetry. Mol Cell Biol. 2011;31(11):2241-52.
36. Li De La Sierra IM, Vincent M, Padron G, Gallay J. Interaction of recombinant human epidermal growth factor with phospholipid vesicles. A steady-state and time-resolved fluorescence study of the bis-tryptophan sequence (TRP49-TRP50). European Biophysics Journal. 1992;21(5):337-44.
37. Hommel U, Harvey TS, Driscoll PC, Campbell ID. Human epidermal growth factor. High resolution solution structure and comparison with human transforming growth factor alpha. J Mol Biol. 1992;227(1):271-82.
38. Puddicombe SM, Chamberlin SG, MacGarvie J, Richter A, Drummond DR, Collins J, et al. The significance of valine 33 as a ligand-specific epitope of transforming growth factor alpha. The Journal of biological chemistry. 1996;271(26):15367-72.
39. Lahti JL, Lui BH, Beck SE, Lee SS, Ly DP, Longaker MT, et al. Engineered epidermal growth factor mutants with faster binding on-rates correlate with enhanced receptor activation. FEBS letters. 2011;585(8):1135-9.
40. Carpenter G, Cohen S. Epidermal growth factor. Annual review of biochemistry. 1979;48:193-216.
41. Lindvall C, Hou M, Komurasaki T, Zheng C, Henriksson M, Sedivy JM, et al. Molecular characterization of human telomerase reverse transcriptase-immortalized human fibroblasts by gene expression profiling: activation of the epiregulin gene. Cancer Res. 2003;63(8):1743-7.

42. Grudinkin PS, Zenin VV, Kropotov AV, Dorosh VN, Nikolsky NN. EGF-induced apoptosis in A431 cells is dependent on STAT1, but not on STAT3. Eur J Cell Biol. 2007;86(10):591-603.
43. Ibuka S, Matsumoto S, Fujii S, Kikuchi A. The P2Y(2) receptor promotes Wnt3a- and EGF-induced epithelial tubular formation by IEC6 cells by binding to integrins. J Cell Sci. 2015;128(11):2156-68.
44. Bjorkelund H, Gedda L, Andersson K. Comparing the epidermal growth factor interaction with four different cell lines: intriguing effects imply strong dependency of cellular context. PloS one. 2011;6(1):e16536.
45. Macdonald-Obermann JL, Pike LJ. Different epidermal growth factor (EGF) receptor ligands show distinct kinetics and biased or partial agonism for homodimer and heterodimer formation. The Journal of biological chemistry. 2014;289(38):26178-88.
46. Innan H, Kondrashov F. The evolution of gene duplications: classifying and distinguishing between models. Nature Reviews Genetics. 2010;11(2):97-108.
47. Zhou J, Liu D, Sa Z, Huang W, Zou Y, Gu X. Effective estimation of the minimum number of amino acid residues required for functional divergence between duplicate genes. Mol Phylogenet Evol. 2017;113:126-38.
48. Laisney J, Braasch I, Walter RB, Meierjohann S, Schartl M. Lineage-specific co-evolution of the Egf receptor/ligand signaling system. BMC Evol Biol. 2010;10:16.
49. Bakker J, Spits M, Neefjes J, Berlin I. The EGFR odyssey – from activation to destruction in space and time. Journal of Cell Science. 2017;130(24):4087-96.
50. Sotelo MJ, García-Paredes B, Aguado C, Sastre J, Díaz-Rubio E. Role of cetuximab in first-line treatment of metastatic colorectal cancer. World journal of gastroenterology. 2014;20(15):4208-19.
51. Zerbino DR, Achuthan P, Akanni W, Amode MR, Barrell D, Bhai J, et al. Ensembl 2018. Nucleic Acids Res. 2018;46(D1):D754-D61.
52. Katoh K, Standley DM. MAFFT Multiple Sequence Alignment Software Version 7: Improvements in Performance and Usability. Mol Biol Evol. 2013;30(4):772-80.
53. Berman HM, Westbrook J, Feng Z, Gilliland G, Bhat TN, Weissig H, et al. The Protein Data Bank. Nucleic Acids Res. 2000;28(1):235-42.
54. Goddard TD, Huang CC, Meng EC, Pettersen EF, Couch GS, Morris JH, et al. UCSF ChimeraX: Meeting modern challenges in visualization and analysis. Protein Sci. 2018;27(1):14-25.
55. Okonechnikov K, Golosova O, Fursov M, Team U. Unipro UGENE: a unified bioinformatics toolkit. Bioinformatics. 2012;28(8):1166-7.
56. Nguyen LT, Schmidt HA, von Haeseler A, Minh BQ. IQ-TREE: A Fast and Effective Stochastic Algorithm for Estimating Maximum-Likelihood Phylogenies. Mol Biol Evol. 2015;32(1):268-74.
57. Kalyaanamoorthy S, Minh BQ, Wong TKF, von Haeseler A, Jermiin LS. ModelFinder: fast model selection for accurate phylogenetic estimates. Nat Methods. 2017;14(6):587-+.
58. Okonechnikov K, Golosova O, Fursov M, team tU. Unipro UGENE: a unified bioinformatics toolkit. Bioinformatics. 2012;28(8):1166-7.
59. Colell EA, Iserte JA, Simonetti FL, Marino-Buslje C. MISTIC2: comprehensive server to study coevolution in protein families. Nucleic Acids Res. 2018;46(W1):W323-w8.
60. Capra JA, Singh M. Predicting functionally important residues from sequence conservation. Bioinformatics. 2007;23(15):1875-82.
61. Puddicombe SM, Wood L, Chamberlin SG, Davies DE. The interaction of an epidermal growth factor/transforming growth factor alpha tail chimera with the human

epidermal growth factor receptor reveals unexpected complexities. The Journal of biological chemistry. 1996;271(48):30392-7.
62. Giard DJ, Aaronson SA, Todaro GJ, Arnstein P, Kersey JH, Dosik H, et al. In vitro cultivation of human tumors: establishment of cell lines derived from a series of solid tumors. J Natl Cancer Inst. 1973;51(5):1417-23.
63. Abraham MJ, Murtola T, Schulz R, Páll S, Smith JC, Hess B, et al. GROMACS: High performance molecular simulations through multi-level parallelism from laptops to supercomputers. SoftwareX. 2015;1-2:19-25.
64. Huang J, MacKerell AD, Jr. CHARMM36 all-atom additive protein force field: validation based on comparison to NMR data. J Comput Chem. 2013;34(25):2135-45.
65. Meng EC, Pettersen EF, Couch GS, Huang CC, Ferrin TE. Tools for integrated sequence-structure analysis with UCSF Chimera. BMC Bioinformatics. 2006;7:339.
66. Waterhouse A, Bertoni M, Bienert S, Studer G, Tauriello G, Gumienny R, et al. SWISS-MODEL: homology modelling of protein structures and complexes. Nucleic Acids Res. 2018;46(W1):W296-W303.
67. Krivov GG, Shapovalov MV, Dunbrack RL, Jr. Improved prediction of protein side-chain conformations with SCWRL4. Proteins. 2009;77(4):778-95.
68. Lemkul JA. From Proteins to Perturbed Hamiltonians: A Suite of Tutorials for the GROMACS-2018 Molecular Simulation Package [Article v1.0]. Living J Comp Mol Sci. 2019; 1(1):5068.
69. Páll S, Hess B. A flexible algorithm for calculating pair interactions on SIMD architectures. Computer Physics Communications. 2013;184(12):2641-50.
70. Hess B, Bekker H, Berendsen HJC, Fraaije JGEM. LINCS: A linear constraint solver for molecular simulations. Journal of Computational Chemistry. 1997;18(12):1463-72.
71. Essmann U, Perera L, Berkowitz ML, Darden T, Lee H, Pedersen LG. A smooth particle mesh Ewald method. The Journal of Chemical Physics. 1995;103(19):8577-93.
72. Humphrey W, Dalke A, Schulten K. VMD: visual molecular dynamics. J Mol Graph. 1996;14(1):33-8, 27-8.
73. Grant BJ, Rodrigues AP, ElSawy KM, McCammon JA, Caves LS. Bio3d: an R package for the comparative analysis of protein structures. Bioinformatics. 2006;22(21):2695-6.

Supplementary material

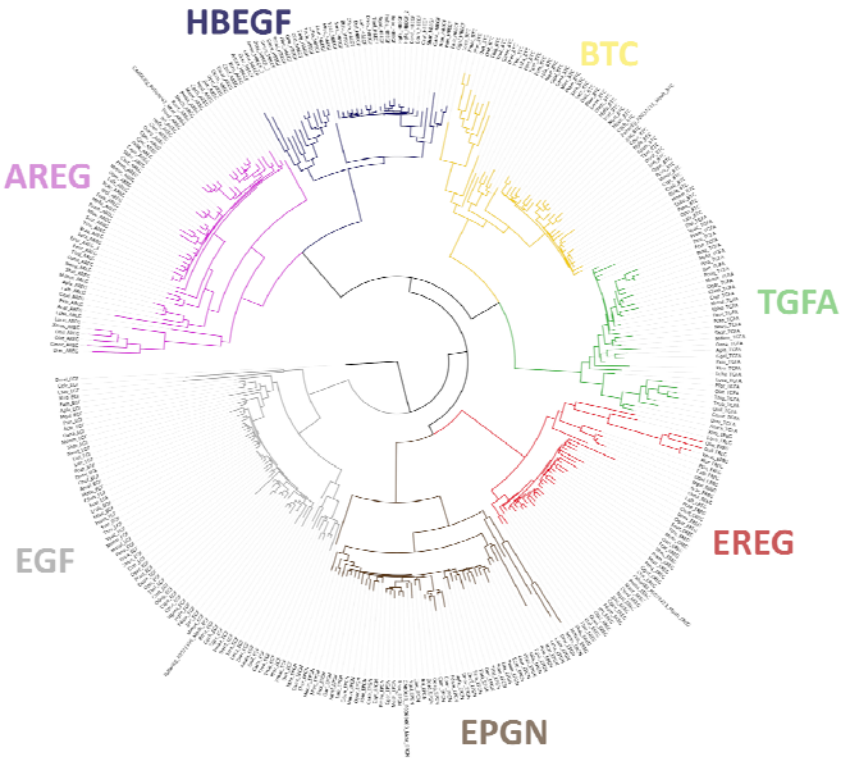

Supplementary figure 1. EGFR ligands orthologs tree. The tree was obtained using Maximum Likelihood algorithm. *C elegans* EGF was used as outgroup. The EGFR ligands cluster neatly. Interestingly, fish ligands are found to have longer branches on average. The tree was made using iqtree ModelFinder. The best-fit model used is JTT+R6.

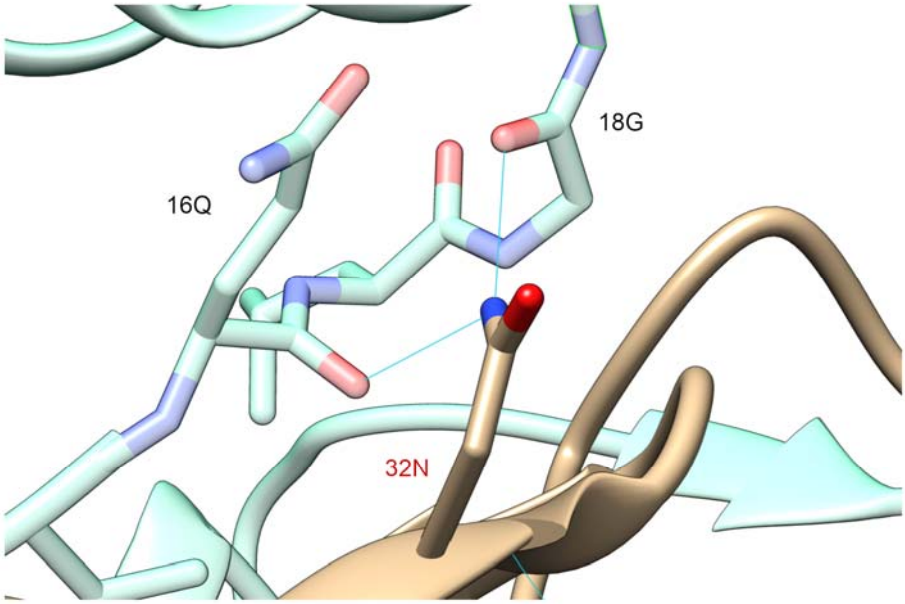

Supplementary figure 2. Crystalized structure of WT EGF with the highlighted position N32, In the interaction with the position Q16 and G18 of the EGFR receptor backbone.

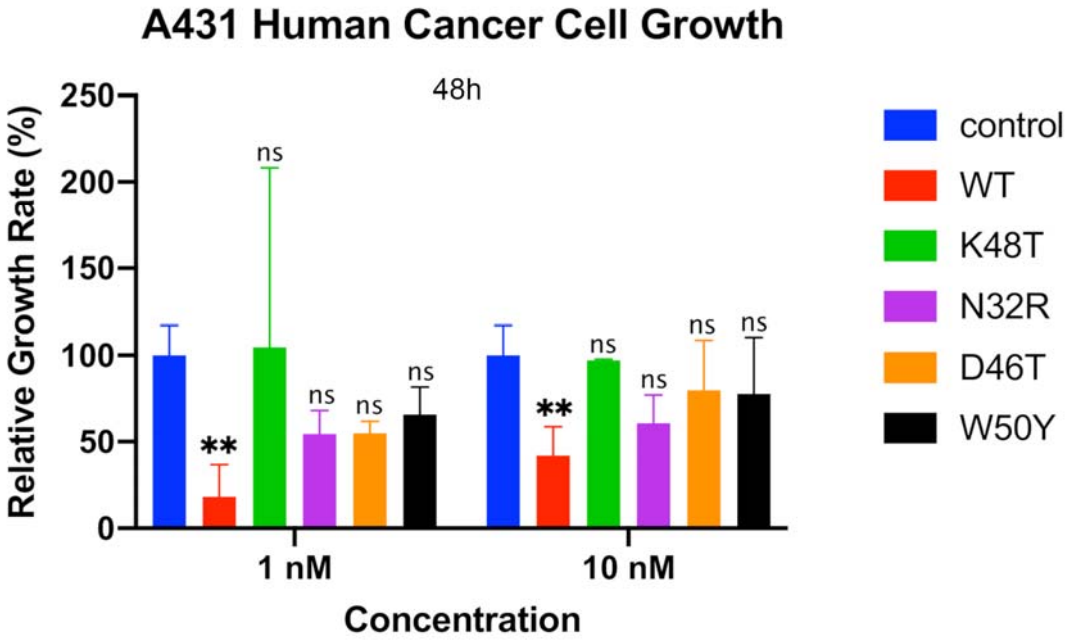

Supplementary figure 3. Effect of 1nM and 10nM concentration of EGF variants on the proliferation of A431 skin cancer cells. The data represent the relative growth percentage to control based on the confluence of cells (mean ± standard deviation) for each concentration of EGF variants. The percentage confluence was estimated 48 h after the treatment (two replicates/treatment).

Supplementary data 1. Time-lapse video of the proliferation of A431 and Bj-5tα cells. Treatment with 100 nM ligand was performed at the 24h mark. Evidences of a balance between differentiation and proliferation are found in the fibroblast, where a reduced proliferation is associated to cellular morphology differences in WT and K48T.